First principles calculation of the phonons modes in the hexagonal YMnO_3 ferroelectric and paraelectric phases

Julien Varignon, Sébastien Petit, Marie-Bernadette Lepetit

▶ **To cite this version:**

Julien Varignon, Sébastien Petit, Marie-Bernadette Lepetit. First principles calculation of the phonons modes in the hexagonal YMnO_3 ferroelectric and paraelectric phases. 2012. hal-00677352

HAL Id: hal-00677352
https://hal.science/hal-00677352

Preprint submitted on 8 Mar 2012

HAL is a multi-disciplinary open access archive for the deposit and dissemination of scientific research documents, whether they are published or not. The documents may come from teaching and research institutions in France or abroad, or from public or private research centers.

L'archive ouverte pluridisciplinaire **HAL**, est destinée au dépôt et à la diffusion de documents scientifiques de niveau recherche, publiés ou non, émanant des établissements d'enseignement et de recherche français ou étrangers, des laboratoires publics ou privés.

First principles calculation of the phonons modes in the hexagonal $YMnO_3$ ferroelectric and paraelectric phases

Julien Varignon,[1] Sébastien Petit,[1] and Marie-Bernadette Lepetit[1]

[1] *CRISMAT, ENSICAEN-CNRS UMR6508, 6 bd. Maréchal Juin, 14050 Caen, FRANCE*

(Dated: February 16, 2012)

The lattice dynamics of the $YMnO_3$ magneto-electric compound has been investigated using density functional calculations, both in the ferroelectric and the paraelectric phases. The coherence between the computed and experimental data is very good in the low temperature phase. Using group theory, modes continuity and our calculations we were able to show that the phonons modes observed by Raman scattering at 1200K are only compatible with the ferroelectric $P6_3cm$ space group, thus supporting the idea of a ferroelectric to paraelectric phase transition at higher temperature. Finally we proposed a candidate for the phonon part of the observed electro-magnon. This mode, inactive both in Raman scattering and in Infra-Red, was shown to strongly couple to the Mn-Mn magnetic interactions.

I. INTRODUCTION

Materials presenting magneto-electric coupling exhibit magnetic properties coupled to the electric properties, such as polarization or dielectric constant. These materials have attracted a lot of attention over the last years since the magneto-electric coupling allows a possible control of the magnetic properties by an electric field and over electric properties using a magnetic field.

Unfortunately, the microscopic origin of the coupling between the magnetic and electric order parameters is still ill known. The knowledge of phonons spectra can however bring help on understanding this coupling. Indeed, not only the phonons modes are strongly related to the existence and amplitude of a spontaneous polarization, but in addition strong spin-phonons coupling occur in multiferroic material. This coupling can even be strong enough in order to result in hybrid excitations built from the mixing between phonons and spin-waves[1]. The existence of such hybrid modes, called electromagnons, were recently discovered in $RMnO_3$ orthorhombic manganites[2] using optical measurements. More recently such excitations were also found by inelastic neutrons scattering in the hexagonal manganite $YMnO_3$[3,4].

Hexagonal $YMnO_3$ is a layered compound where the manganese ions are located in triangle-based bipyramids. These bipyramids are arranged in planes parallel to the $(\vec{a},\vec{b})$ direction so that the manganese ions form a distorted triangular lattice (see figure 1). They share an oxygen atom in the $(\vec{a},\vec{b})$ planes. The yttrium atom is located in between the bipyramids layers. $YMnO_3$ is paraelectric at high temperature with space group $P6_3/mmc$. Under a critical temperature it is ferroelectric, with space group $P6_3cm$; the polarization is aligned along the $\vec{c}$ direction. The temperature of this paraelectric (PE) to ferroelectric (FE) phase transition is however still under debate. Indeed, usually assumed to be around $\simeq 920\,K$[5], it was recently proposed to occur at a higher temperature, $\simeq 1050-1100\,K$[6,7]. A very recent neutrons diffraction investigation[8] suggests the existence of an iso-symmetric phase transition at $\simeq 920\,K$, resulting in a strong lowering of the polarization amplitude, while the non-centrosymmetric to centrosymmetric transition occurs at $1258 \pm 4\,K$ only. At much lower temperature ($T_N \simeq 75\,K$) $YMnO_3$ undergoes a paramagnetic (PM) to antiferromagnetic (AFM) transition. The Mn^{3+} ions are in a high spin state $S=2$. Neutrons diffraction experiments witness an in-plane spins orientation associated with a 120° ordering, with the spins perpendicular to the Mn–O bonds[9,10]. The ferroelectric and antiferromagnetic order parameters are coupled and a giant atomic motion was revealed at the Néel temperature[11]. The magnetic transition is however an iso-structural transition and the space group remains $P6_3cm$ in the AFM phase[10]. The magnetic space group is more subject to caution. Indeed, while most authors favor an identical $P6_3cm$ magnetic and structural space group[9,10], the absence of a linear magneto-electric coupling and the existence of a ferromagnetic component recently observed[4,12] are incompatible with the $P6_3cm$ magnetic group. Group analysis shows that these experimental data can only be accounted for in the $P6_3'$ magnetic group[12].

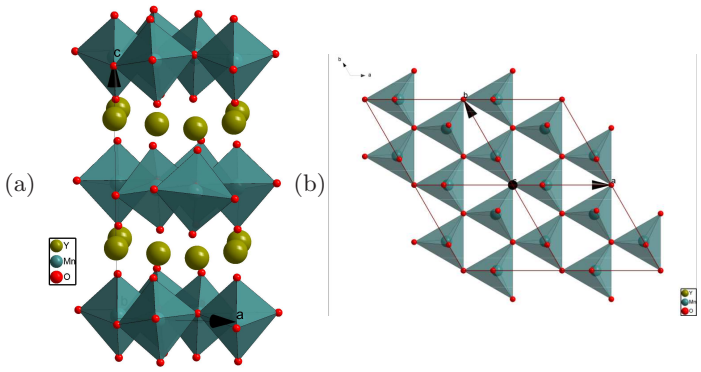

Figure 1: (a) representation of the $YMnO_3$ crystal structure. (b) view along the $\vec{c}$ direction of the MnO_5 bipyramids layers.

Phonons spectra are often used to help understanding both the ferroelectric/paraelectric transitions and the magneto-electric coupling. While the $YMnO_3$ phonons

spectrum has been experimentally studied both by Raman[13–15] and Infra-Red[16] measurements, there is still many opened questions concerning not only modes assignations but also the fact that several of the symmetry allowed modes are not experimentally observed. First principle calculations not only could help understanding the experimental observation but also could yield more light on the recently observed electromagnon[3,4]. The present paper thus presents first principle calculations of the $YMnO_3$ phonons spectrum in the different space groups associated with the FE and PE phases, that is $P6_3cm$ and $P6_3/mmc$. The next section will be devoted to the methodological details and preliminary results (geometry optimization, Born effective charges, polarization, dielectric tensor, etc...) and section III will describe and discuss phonons results.

II. METHOD AND PRELIMINARY RESULTS

We performed geometry optimization, spontaneous polarization and phonons frequencies calculations within the Density Functional Theory (DFT) as implemented in the Crystal09 package[17]. Since the manganese 3d shells are strongly correlated we used hybrid functionals in order to better take into account the self-interaction cancellation. Three different functionals were used in this work, namely the classical B3LYP functional[18], the recently developed B1WC[19] functional for ferroelectric systems and a B1PW[19] functional corresponding to the B1WC one with the Perdew-Wang exchange functional[20]. Only the B1PW results are presented in the paper, the results obtained with the other functionals can be found in the supplementary data. Small core pseudo-potentials were used for the heavy atoms (Mn and Y) associated with semi-valence and valence 2ζ and 2ζ plus polarization basis sets[21]. The oxygen ions are represented in an all-electrons basis set of 2ζ quality specifically optimized for O^{2-} ions[21]. The mono-determinantal character of the Kohn-Sham approximation does not allow the possibility to deal with magnetic frustration as observed in $YMnO_3$. Indeed, only collinear magnetism is possible in the CRYSTAL code. A non-magnetic electronic density can be calculated, however it does not account for the open-shell and high spin character of the Mn^{3+} ions, which are responsible for a large stabilization energy (of the order of two Hubbard $3d$-shell U per Mn atom, this is of the order of 10eV) and crucial for a reasonable electronic structure representation. A "*pseudo*" antiferromagnetic configuration can be proposed on a $2\times2\times1$ cell. In this case, only two among the three antiferromagnetic (AFM) couplings are satisfied within each triangle. It results in a lower energy for the antiferromagnetic bonds and an associated loss of symmetry. When the geometry optimization is performed, the Mn-Mn distances associated with anti-aligned spins are shorter than the bonds with aligned spins, resulting in a structure with unphysical symmetry and characteristics. The choice of a ferromagnetic (FM) configuration for the Mn^{3+} S=2 spins thus seems the best compromise. Indeed, not only this configuration respects the system symmetry (a crucial aspect for accurate phonons modes), but also the energy error that can be associated with the loss of the inter-atomic exchange energy (that is $1/2J \simeq 1.5\,\text{meV}$ per bond) is much weaker than the error associated with the loss of the magnetic character for the Mn^{3+} ions. For these reasons all our calculations will be done within a ferromagnetic Mn spins alignment.

Within this procedure, we computed the polarization (using Berry phase approach) for the different experimental geometries available in the literature at different temperatures. Table I reports the computed polarization values. One sees immediately that our computed values are in very good agreement with the experimental ones, despite the fact that the magnetic order used in the calculation is ferromagnetic and not antiferromagnetic. The quality of these results thus validate our choices for the calculations. In addition it supports the idea, first proposed by Lee *et al*[11], that in this system the magneto-electric coupling is mainly driven by elastic effects rather than by a direct coupling between the polarization and the magnetic order.

Structures	10 K[11]	180 K[22]	300 K[11]
Exp. P_S	~ 1[12]	6.2[23]	4.5[24]
This work	1.1	6.2	4.9

Table I: Spontaneous polarization P_S in $\mu C.cm^{-2}$ for different temperatures. Experimental and computed values using the experimental geometries at the given temperatures.

In a second step we optimized the geometry. Both the cell parameters and the atomic positions compare very well with the experimental values in the paramagnetic phase[22]. Indeed, the error on the lattice parameters is weaker than 0.5% and for the atomic positions $\sum_{at}|\vec{r}^{\,exp}_{at} - \vec{r}^{\,calc}_{at}|^2 = 0.0087\,\text{Å}^2$.

Finally we computed the Born effective charge tensor $Z^\star$ for the optimized geometry. They are reported in table II. Again our results compare well with the experimental evaluations validating our methodological choices.

III. THE PHONONS SPECTRA

Table III displays the Γ point optical transverse (TO) phonon modes, both for the paraelectric (columns 1-2) and ferroelectric (columns 6-7) phases. Raman and Infra-Red (IR) experimental data are given for comparison. The $P6_3/mmc$ group of the paraelectric phase decomposes in

$$1A_{1g} \oplus 3A_{2u} \oplus 3B_{1g} \oplus 2B_{2u} \oplus 1E_{1g} \oplus 3E_{1u} \oplus 3E_{2g} \oplus 2E_{2u}$$

optical modes, out of which the A_{1g}, E_{1g} and E_{2g} are Raman active while the A_{2u} and E_{1u} are IR active, leaving the B_{1g}, B_{2u} and E_{2u} modes inactive both in Raman

Z^*		x	y	z	Dynamic charge Exp. [16]	Dynamic charge This work
	x	3.5	0.0	0.0		
Y_1	y	0.0	3.5	0.0	4.0	3.6
	z	0.0	0.0	3.9		
	x	3.5	0.0	0.0		
Y_2	y	0.0	3.5	0.0	4.0	3.6
	z	0.0	0.0	3.9		
	x	3.1	0.2	-0.4		
Mn	y	0.2	3.4	0.2	4.0	3.5
	z	0.2	-0.1	4.0		
	x	-2.0	0.1	0.3		
O_1	y	0.1	-1.9	-0.1	-2.7	-2.3
	z	-0.1	0.1	-3.1		
	x	-2.0	0.2	0.2		
O_2	y	0.2	-1.8	-0.1	-2.7	-2.3
	z	-0.1	0.1	-3.3		
	x	-2.9	0.0	0.0		
O_3	y	0.0	-2.9	0.0	-2.7	-2.5
	z	0.0	0.0	-1.6		
	x	-2.9	-0.2	0.0		
O_4	y	0.2	-2.9	0.0	-2.7	-2.5
	z	0.0	0.0	-1.5		

Table II: Born effective charge. The dynamic charge, $Tr(Z^\star)/3$, is compared to the experimental evaluation from infra-red measurements[16].

and IR. The $P6_3cm$ group of the ferroelectric phase decomposes in

$$9A_1 \oplus 5A_2 \oplus 5B_1 \oplus 10B_2 \oplus 14E_1 \oplus 15E_2$$

optical modes, out of which the A_1, E_1 are active both in Raman and IR, the E_2 are active in Raman only and the A_2, B_1 and B_2 are inactive both in Raman and IR.

For the ferroelectric phase, the optical longitudinal (LO) phonon modes have also been evaluated and are reported in the supplementary data.

A. High temperature discussion

At high temperature only four modes were experimentally measured by Fukumura *et al*[14]. These modes were respectively assigned by Fukumura *et al* to one A_{1g} mode ($666\,\mathrm{cm}^{-1}$), one E_{1g} mode ($420\,\mathrm{cm}^{-1}$) and two E_{2g} modes (120 and $395\,\mathrm{cm}^{-1}$) of the $P6_3/mmc$ group of the high temperature PE phase. In addition figure 5 of reference 14 clearly shows that these modes are observed continuously from 300 K to 1200 K in the same energy ranges. Going back to our calculations, if we want to assign these modes by continuity from the low temperature phase ($P6_3cm$ to $P6_3/mmc$), we have to suppose that the mode at $395\,\mathrm{cm}^{-1}$ should be assigned as E_{2u} (computed at $402\,\mathrm{cm}^{-1}$ in the $P6_3/mmc$ group and at $392\,\mathrm{cm}^{-1}$ in the $P6_3cm$ group, and measured at $406\,\mathrm{cm}^{-1}$ in the low temperature phase) and not as E_{2g} (computed at $500\,\mathrm{cm}^{-1}$ in the $P6_3/mmc$ group and at $473\,\mathrm{cm}^{-1}$ in the $P6_3cm$ group, and measured at $483\,\mathrm{cm}^{-1}$ in the low temperature phase). Similarly, the mode at $420\,\mathrm{cm}^{-1}$ should be assigned as E_{1u} and not as E_{1g} and the mode at $120\,\mathrm{cm}^{-1}$ should be assigned as E_{2u} rather than E_{2g}. At this point there is a clear contradiction between the continuity requirement of the phonons modes between the low and high temperature phase and the Raman symmetry requirements. Indeed the "ungerade" E_{1u} and E_{2u} irreducible representations (irreps) are not Raman active and no crystal disorientation or twinning could induce an inversion between a "gerade" and an "ungerade" mode. We must thus assume that the symmetry group at 1200 K cannot be the $P6_3/mmc$ group.

What type of hypotheses are left? The first possibility is the existence of an intermediate phase in the 1200 K temperature range as suggested by several authors[7,25,26]. However the $P6_3/mcm$ symmetry group suggested is no more than the $P6_3/mmc$ group, compatible with the phonons spectrum. Indeed, symmetry group analysis shows that the $P6_3/mmc$ to $P6_3/mcm$ transformation only exchange the B_{1g} with the B_{2g}, and the B_{1u} with the B_{2u} irreps. A second possibility would be that the intermediate phase corresponds to the $P6_3mc$ group. In this group the inversion center is lost, and the E_{1g} and E_{1u} irreps of $P6_3/mmc$ are associated with the E_1 irrep of the $P6_3mc$ group and with the E_1 irrep of the low temperature phase (resp. E_{2g} and E_{2u} are associated with E_2). Both the E_1 and E_2 irreps are Raman active in the $P6_3mc$ group and the experimental Fukumura *et al*[14] data can be easily associated with the computed modes (see table III, columns 3-4). The average error between the computed and measured frequencies is $18\,\mathrm{cm}^{-1}$, essentially supported by the higher A mode ($3\,\mathrm{cm}^{-1}$ for all the other modes). The main problem with this hypothesis is that the unit cell tripling at the $P6_3mc$ to $P6_3cm$ transition should have been seen in diffraction experiments, while it does not seem to be the case[25]. Therefore, the only possibility compatible with all data seems to be that a $P6_3/mmc$ to $P6_3cm$ phase transition occurs at a temperature higher than 1200 K, as proposed by Jeong[27] and Gibbs[8] from neutrons diffraction measurements ($T_c = 1258\,\mathrm{K} \pm 14\,\mathrm{K}$). In other terms, all the high temperature data from Fukumura *et al*[14] should be interpreted within the ferroelectric $P6_3cm$ group.

B. Low temperature discussion

At low temperature our computed modes fit quite well with the available experimental data, both Raman and IR (see table III, columns 6 and further). Table IV displays the average errors between our computed modes and the experimental data for each irreducible representation. The experimental phonons modes can be associated with the computed ones except for a few exceptions. i) The mode at $190\,\mathrm{cm}^{-1}$ seen by Iliev *et al* in the A_1 irreducible representation cannot be associated with a computed mode. This mode, not seen by the other authors,

This work				Raman	This work		IR			Raman		
$P6_3/mmc$		$P6_3mc$		Fukumura [14]	$P6_3cm$		Zaghrioui [16]		Iliev [13]	Fukumura [14]	Vermette [15]	
Irrep	TO	Irrep	TO	1100 K	Irrep	TO	10 K	300 K	300 K	15 K	10 K	300 K
					A_2	33						
E_{2u}	121	E_2	121	120	E_2	119			135	141	-	-
B_{1g}	187	B	179		B_2	136						
					B_1	147						
E_{2g}	159	E_2	148		E_2	150			**190**	-	-	-
A_{2u}	109	A	138		A_1	186	163	154	148	160	161	151
E_{1u}	187	E_1	177		E_1	186	167	162	-	-	-	-
					E_1	211	211	207	-	**210**	-	-
					E_2	213			215	-	-	-
B_{2u}	211	B	204		B_2	218						
					B_2	233						
E_{2g}	257	E_2	235		E_2	233			-	225	231	223
E_{1u}	264	E_1	241		E_1	238	257	249	-	247	-	-
					A_2	241						
					A_1	262	239	235	-	-	244	241
					E_1	269	-	-	-	-	-	-
					E_2	270			-	-	-	-
					B_1	276						
					B_2	289						
					A_1	292	266	260	257	264	264	259
					E_2	294			302	307		
					B_1	302						
					E_1	303	301	299	-	-	-	-
					E_1	326	-	-	-	-	-	-
					A_2	333						
					A_1	334	311	304	297	-	307	300
					E_2	335			-	331	-	-
					B_2	369						
					E_2	383			-	-	357	356
					E_1	386	-	-	-	360	361	354
E_{2u}	402	E_2	402	395	E_2	392			-	406	-	-
					E_1	404	381	380	376	377	-	-
					B_2	430						
					E_2	434			-	444	441	439
					E_1	437	409	400	408	-	-	-
E_{1u}	426	E_1	421	420	E_1	451	423	416	-	420	-	-
					E_2	454			-	-	-	-
					B_1	458						
E_{1g}	483	E_1	471		E_1	461	-	-	-	509	-	-
					A_2	462						
					A_1	465	-	-	-	-	-	-
E_{2g}	500	E_2	484		E_2	473			-	483	-	-
A_{2u}	518	A	467		A_1	492	434	432	433	435	434	431
B_{1g}	495	B	457		B_2	504						
					E_2	515			-	-	-	-
					E_1	515	-	-	-	-	-	-
					A_1	534	489	486	459	466	467	461
					B_1	552						
					A_2	561						
					B_2	567						
A_{2u}	611	A	600		A_1	612	565	562	-	-	-	-
					E_2	643			-	647	-	-
					E_1	643	594	594	-	-	-	-
					E_2	667			-	-	-	-
					E_1	668	-	-	632	638	637	631
A_{1g}	771	A	735	666	A_1	722	-	-	681	686	686	683
B_{2u}	772	B	729		B_2	728						
B_{1g}	868	B	827		B_2	813						

Table III: Hexagonal $YMnO_3$ vibrational frequencies in cm^{-1} for the paraelectric ($P6_3/mmc$) and ferroelectric ($P6_3cm$) phases. The frequencies for one of the possible intermediate phases ($P6_3mc$) was also computed. Modes with problematic assignment are in bold faces ; modes that are symmetry allowed but not seen are designed by dashes.

Irrep	IR			Raman		
	Zaghrioui [16]		Iliev [13]	Fukumura [14]	Vermette [15]	
	10 K	300 K	300 K	15 K	10 K	300 K
A_1	14	16	20	21	15	17
E_1	8	8	18	11	19	24
E_2			11	4	9	10

Table IV: Average errors per irrep on the $YMnO_3$ vibrational frequencies compared to different experimental data (in cm^{-1}).

cannot be associated with a A_1 mode. Indeed, the A_1 modes are IR active and all predicted modes are observed by Zaghrioui *et al*[16] up to more than 450 wave numbers. If not artifactual, the 190 cm^{-1} mode must belong to another irreducible representation. The only possibility in this energy range is an E_2 mode predicted at 150 cm^{-1}. Indeed, all other IR or Raman active modes in this energy range are experimentally observed and easily associated with the computed phonons. ii) The 210 cm^{-1} A_1 mode seen by Fukumura *et al*[14]. Once again a A_1 mode around 210 cm^{-1} is incompatible both with the computed values and with the other experimental results (IR or Raman). Most probably this mode has been improperly assigned as a A_1 mode and should rather be considered as a E_1 (seen at 211 cm^{-1} by Zaghrioui *et al*[16]) or a E_2 mode (seen at 215 cm^{-1} by Iliev *et al*[13]).

Another point we would like to address is the reason why all phonons modes are not observed in experimental data. As far as the IR active modes are concerned we computed an estimate of the intensities, the analysis of which gives us some insight on the reasons some modes are not observed. In the A_1 representation two modes are not seen in reference 16, namely the highest mode computed around 720 cm^{-1} and the mode computed around 460 cm^{-1}. The IR computed intensity of the 720 cm^{-1} A_1 mode is very weak (between 5 and 12 km/mol according to the functional used) and it is thus not surprising this mode is not seen experimentally. The IR intensity of the A_1 mode computed around 460 cm^{-1} mode is of the same order of magnitude as the next computed A_1 mode at 492 cm^{-1} which was associated to the experimental mode found at 434 cm^{-1}). Even if the IR intensity remains small it is non negligible and the second mode is observed. Assuming an equivalent shift in energy between experiments and calculation on these two modes, the first mode should be searched around 400 cm^{-1} in the IR spectrum however it is not seen. In the E_1 irreducible representation, five modes are not seen in IR experiments, namely the modes computed at 269 cm^{-1}, 386 cm^{-1}, 461 cm^{-1}, 515 cm^{-1} and 668 cm^{-1}. The calculations reveals that all these modes are associated with very low IR intensities that could explain there are not seen by Zaghrioui *et al*[16].

C. The A_2 phonon mode at 33 cm^{-1}

We would now like to discuss in a little more details the first optical mode, computed at 33 cm^{-1} $\simeq$ 4 meV in the A_2 irreducible representation. The displacements vector associated with this phonon mode is reported on table V and pictured in figure 2.

Atom	Positions			Displacements		
	x	y	z	x	y	z
Y_1	0.0000	0.0000	z_{Y_1}	0.0000	0.0000	0.0000
Y_2	1/3	−1/3	z_{Y_2}	0.0000	0.0000	-0.0713
Mn_1	x_{Mn_1}	0.0000	z_{Mn_1}	0.0322	0.0558	0.0000
O_1	x_{O_1}	0.0000	z_{O_1}	0.0206	0.0357	0.0000
O_2	x_{O_2}	0.0000	z_{O_2}	0.0272	0.0471	0.0000
O_3	0.0000	0.0000	z_{O_3}	0.0000	0.0000	0.0000
O_4	1/3	2/3	z_{O_4}	0.0000	0.0000	-0.0145

Table V: Displacements vector (normalized to classical amplitudes) associated with the first A_2 mode found around 33 cm^{-1}.

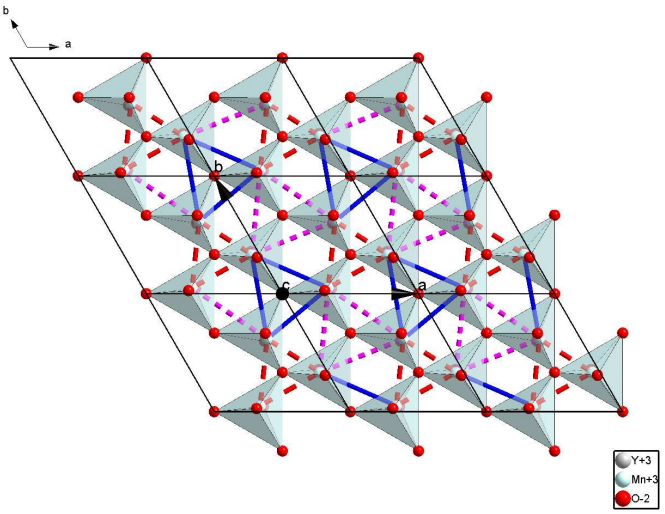

Figure 2: (Color online) Schematic picture of the atomic displacements in the $(\vec{a}, \vec{b})$ plane for the lowest A_2 phonon mode. The blue, solid lines, Mn triangles remain nearly untouched and rotate as a whole around the $\vec{c}$ axis. The red, dashed and magenta, dotted Mn triangles are alternatively enlarged/reduced, the Mn ions moving within the $(\vec{a}, \vec{b})$ plane while the central oxygens move conversely along the $\vec{c}$ direction. A jmol xyz file can be found in the supplementary data in order to visualize the displacements of one manganese plane.

This phonon mode, active neither in Infra-Red nor in Raman experiments exhibits displacements that can be expected to strongly affect the magnetic exchange coupling constants along the red, dashed and magenta, dotted bonds as picture in figure 2.

Let us notice that the effective exchange J between two manganese atoms is the sum of a direct exchange contribution J_d (Pauli exchange, always ferromagnetic,

exponentially dependent on the Mn-Mn distance) and a through-ligand super-exchange term J_l (antiferromagnetic, dependent on the metal ligand distances and on the Mn-O-Mn angles). In $YMnO_3$ the magnetic exchange couplings are known to be antiferromagnetic showing that the through-ligand super-exchange term J_l dominates over the direct exchange contribution J_d. We analyzed this super-exchange term and reported in figure 3 the main super-exchange paths. J_l thus scales as the sum of the four associated super-exchange terms, each of them scaling as the square of the product of the associated $Mn_1 3d - O2p$ orbital overlap and the $O2p - Mn_2\, 3d$ orbital overlap.

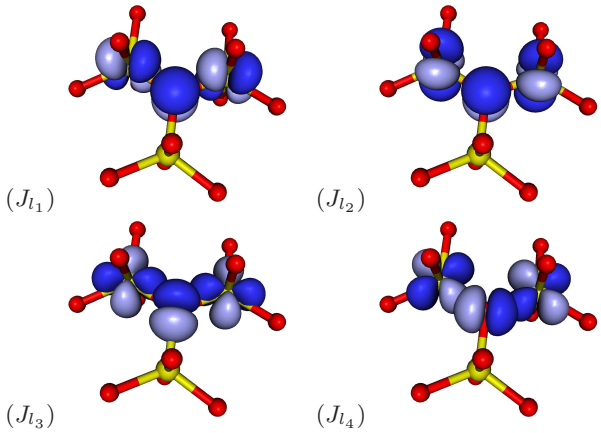

Figure 3: Main super-exchange paths between two manganese atoms. Let us remember that in $YMnO_3$ the manganese is $3d^4$ and the singly occupied orbitals are d_{xy}, $d_{x^2-y^2}$, d_{xz}, d_{yz} if z is along the $\vec{c}$ axis. We can evaluate
$J_{l_1} \sim \langle Mn_1 d_{xz}|Op_z\rangle^2 \langle Op_z|Mn_2 d_{xz}\rangle^2$
$J_{l_2} \sim \langle Mn_1 d_{yz}|Op_z\rangle^2 \langle Op_z|Mn_2 d_{yz}\rangle^2$
$J_{l_3} \sim \langle Mn_1 d_{x^2-y^2}|Op_y\rangle^2 \langle Op_y|Mn_2 d_{x^2-y^2}\rangle^2$
$J_{l_4} \sim \langle Mn_1 d_{xy}|Op_x\rangle^2 \langle Op_x|Mn_2 d_{xy}\rangle^2$

The A_2 phonon mode under consideration involves the following atomic displacements on the red, dashed and magenta, dotted Mn triangles (see figure 2).

- The Mn-Mn bond length elongation / contraction (in opposite phases between red and magenta triangles). This movement affects the direct part of the exchange : J_d, increasing its ferromagnetic character when the Mn-Mn distances are contracted and decreasing it when the Mn-Mn distances are elongated.

- The up and down movement (along the c direction) of the oxygens atoms at the center of these triangles. This movement strongly affects both the Mn-O distances, reducing them when the oxygens come closer to the Mn plane, and the Mn-O-Mn angle.

One sees immediately using figure 3 that, when the oxygen comes closer to the Mn plane, the overlap between the magnetic orbitals of the Mn atoms and the $2p$ bridging orbitals of the central oxygen increases, thus increasing the antiferromagnetic character of J_l. At the same time the Mn-Mn bond length increases thus decreasing the ferromagnetic character of J_d. Both terms goes in the same direction resulting in a enlarged antiferromagnetic character for the bonds of the (alternatively red/magenta) triangles when the central oxygen comes closer to the Mn plane and a reduced antiferromagnetic character when the central oxygen goes away from the Mn plane.

The blue, solid line, Mn triangles (centered around the unit cell origin) are subject to a rotation *as a whole* around the $\vec{c}$ axis going through their central oxygen (O_3). One thus does not expect the magnetic exchange within the blue Mn triangles to be affected by this A_2 phonon mode. However this rotation results in a strong distortion of the triangles with blue red and magenta bond inducing a magnetic interaction scheme quite far from the nearly homogeneous triangular lattice of the static structure.

The main conclusion of this analysis is that this A_2 phonon mode is strongly coupled to the magnetic interactions.

Let us now put these results into perspective with the characteristics of the hybrid phonon-magnon excitation, studied using inelastic polarized and non-polarized neutron scattering by Pailhès and coworkers[4]. One notices that this A_2 mode seems to fulfill all the requirements for a good candidate for the phonon participating to the hybrid mode. Indeed, it is an optical mode in the adequate energy range, exhibiting atomic displacements consistent with the umbrella motion proposed in reference 4 and that can be expected from the above analysis to be strongly coupled to the spin degree of freedom.

IV. CONCLUSION

The present paper proposes Γ point phonon calculations for the $YMnO_3$ compound both in the ferroelectric phase and in the paraelectric phase. Our calculations agrees well with the Infra-Red and Raman experimental data. The experimental versus calculated modes correspondence is discussed in details for the few problematic modes. We were able to explain the fact that several modes could not be seen in IR experiments due to their very low (calculated) intensities. A careful analysis of the phonons modes correspondence, when going from the ferroelectric to the paraelectric phase, is performed and leads to the conclusion that, the phonon modes observed in Raman scattering at 1200K[14] cannot be associated with the paraelectric phase $P6_3/mmc$ space group. The different intermediate subgroups allowed between the paraelectric $P6_3/mmc$ space group and the ferroelectric $P6_3cm$ group were also checked against the modes continuity and the experimental data and had to be discarded. The only possibility agreeing

with the phonon calculations and the experimental data is that the $P6_3/mmc$ to $P6_3cm$ phase transition occurs at a temperature higher than 1200 K, supporting the proposition of Jeong[27] and Gibbs[8] ($T_c = 1258\,\mathrm{K} \pm 14\,\mathrm{K}$).

Finally we studied in more details the first optical mode. This mode belongs to A_2 irreducible representation and is inactive both in IR and Raman experiment. This mode however seems to have all necessary characteristics to be a good candidate for the phonon part of the electro-magnon mode observed in inelastic neutrons scattering by Petit, Pailhès *et al*[3,4].

Acknowledgments

The authors thank V. TaPhuoc and Ph. Ghosez and collaborators for helpful discussions. This work was done with the support of the French national computer center IDRIS under project n○ 081842 and the regional computer center CRIHAN under project n○ 2007013.

[1] V. G. Baryaktar and I. E. Chapius, Sov. Phys. Solid State **11**, 2628 (1970) ; I. A. Akhiezer and L. N. Davydov, Sov. Phys. Solid State **12**, 2563 (1971).
[2] A. Pimenov, A. A. Mukhin, V. YU. Ivanov, V. D. Travkin, A. M. Balbashov and A. Loidl, Nature Physics **2**, 97 (2006).
[3] S. Petit, F. Moussa, M. Hennion, S. Pailheès, L. Pinsard-Gaudart and A. Ivanov, Phys. Rev. Letters **99**, 266604 (2007).
[4] S. Pailhès, X. Fabrèges, L. P. Régnault, L. Pinsard-Godart, I. Mirebeau, F. Moussa, M. Hennion and S. Petit, Phys. Rev. **B 79**, 134409 (2009).
[5] G. A. Smolenskii and I. E. Chupis, Sov. Phys. Usp. **25**, 475 (1982).
[6] T. Katsufuji, M. Masaki, A. Machida, M. Moritomo, K. Kato, E. Nishibori, M. Takata, M. Sakata, K. Ohoyama, K. Kitazawa and H. Takagi, Phys. Rev. **B 66**, 134434 (2002).
[7] S. Abrahams, Acta Crys. **B 65**, 450 (2009).
[8] A. S. Gibbs, K. S. Knight and Ph. Lightfoot, Phys. Rev. **B 83**, 094111 (2011).
[9] E. F. Bertaut, R. Pauthenet and M. Mercier, Physics Letters **7**, 110 (1963).
[10] A. Muñoz, J. A. Alonso, M. J. Martínez-Lope, M. T. Casáis, and J. L. Martínez and M. T. Fernández-Díaz, Phys. Rev. **B 62**, 9498 (2000).
[11] S. Lee, A. Pirogov, M. Kang, K.-H. Jang, M. Yonemura, T. Kamiyama, S.-W. Cheong, F. Gozzo, N. Shin, H. Kimura, Y. Noda and J.-G. Park, Nature **451** 805, (2008).
[12] K. Singh, N. Bellido, Ch. Simon, J. Varignon and M.-B. Lepetit, to be published elsewhere.
[13] M. N. Iliev, H.-G. Lee, V. N. Popov, M. V. Abrashev, A. Hamed, R. L. Meng, and C. W. Chu, Phys. Rev. **B 56**, 2488 (1997).
[14] H. Fukumura, S. Matsui, H. Harima, K. Kisoda, T. Takahashi, T. Yoshimura and N. Fujimura, J. Phys.: Condens. Matter **19** 365239 (2007).
[15] J. Vermette, S. Jandl, A. A. Mukhin, V. Yu Ivanov, A. Balbashov, M. M. Gospodinov and L. Pinsard-Gaudart, J. Phys.: Condens. Matter **22**, 356002 (2010).
[16] M. Zaghrioui, V. Ta Phuoc, R. A. Souza, and M. Gervais, Phys. Rev. **B 78**, 184305 (2008).
[17] R. Dovesi, R. Orlando, B. Civalleri, C. Roetti, V.R. Saunders, C.M. Zicovich-Wilson, Z. Kristallogr. **220**, 571 (2005) ; R. Dovesi, V.R. Saunders, C. Roetti, R. Orlando, C. M. Zicovich-Wilson, F. Pascale, B. Civalleri, K. Doll, N.M. Harrison, I.J. Bush, Ph. D'Arco, M. Llunell, *CRYSTAL09 User's Manual*, University of Torino, Torino, (2009).
[18] A. D. Becke, Phys. Rev. A, **38**, 3098 (1988).
[19] D. I. Bilc, R. Orlando, R. Shaltaf, G. M. Rignanese, J. Iñiguez and P. Ghosez, Phys. Rev. B, **77**, 165107 (2008).
[20] J. P. Perdew and Y. Wang, Phys. Rev. B, **33**, 8800 (1986).
[21] Mn and Y : P. J. Hay and W. R. Wadt, J. Chem. Phys. **82**, 299 (1985); Evarestov et al., Solid State Commun. **127**, 367 (2003).
O : A. Gellé and C. calzado, private communication.
[22] B. B. van Aken, A. Meetsma and Th. T. M. Palstra, Acta Cryst. **C 57**, 230 (2001).
[23] B. B. van Aken, T. T. M. Palstra, A. Filippetti and N. A. Spaldin, Nature Materials **3**, 164 (2004).
[24] S. H. Kim, S. H. Lee, T. H. Kim, T. Zyung, Y. H. Jeong and M. S. Jang, Crys. Res. Tech. **35**, 19 (2000).
[25] G. Nénert, Y. Ren, H. T. Stokes and T. T. M. Palstra, arXiv:cond-mat/0504546.
[26] G. Nénert, M. Pollet, S. Marinel, G. R. Blake, A. Meetsma and T. T. M. Palstra, J. Phys.: Condens. Matter **19**, 466212 (2007).
[27] Il-Kyoung Jeong, N. Hurb and Th. Proffen, J. Appl. Cryst. **40**, 730 (2007).